Article

Journal of
Biomedical Nanotechnology
Vol. 17, 1812–1823, 2021
www.aspbs.com/jbn

Strontium-Loaded Nanotubes of Ti–24Nb–4Zr–8Sn Alloys for Biomedical Implantation

Fei Liu[1, †], Xinyu Wang[2, †], Shujun Li[3], Yiheng Liao[1], Xinxin Zhan[4], Anqi Tao[1], Fu Zheng[5], Huazhi Li[5], Yucheng Su[6], Jiuhui Jiang[5, *], and Cuiying Li[1, *]

[1] *Central Laboratory, Peking University School and Hospital of Stomatology, Beijing, 100081, China*
[2] *Jiamusi University Affiliated Stomatological Hospital, Heilongjiang Key Laboratory of Oral Biomedical Materials and Clinical Application, Jiamusi, 154000, China*
[3] *Titanium Alloy Laboratory, Institute of Metal Research, Chinese Academy of Sciences, Shenyang, 110016, China*
[4] *Department of Dental Materials, Peking University School and Hospital of Stomatology, Beijing, 100081, China*
[5] *Department of Orthodontics, Peking University School and Hospital of Stomatology, Beijing, 100081, China*
[6] *Dental Implant Center, Peking Union Medical College Hospital, Chinese Academy of Medical Sciences, Beijing, 100032, China*

Ti–24Nb–4Zr–8Sn (Ti2448) alloys, with a relatively low elastic modulus and unique mechanical properties, are desirable materials for oral implantation. In the current study, a multifaceted strontium-incorporating nanotube coating was fabricated on a Ti2448 alloy (Ti2-NTSr) through anodization and hydrothermal procedures. *In vitro*, the Ti2-NTSr specimens demonstrated better osteogenic properties and more favorable osteoimmunomodulatory abilities. Moreover, macrophages on Ti2-NTSr specimens could improve the recruitment and osteogenic differentiation of osteoblasts. *In vivo*, dense clots with highly branched, thin fibrins and small pores existed on the Ti2-NTSr implant in the early stage after surgery. Analysis of the deposition of Ca and P elements, hard tissue slices and the bone-implant contact rate (BIC%) of the Ti2-NTSr implants also showed superior osseointegration. Taken together, these results demonstrate that the Ti2-NTSr coating may maximize the clinical outcomes of Ti2448 alloys for implantation applications.

KEYWORDS: *Ti–24Nb–4Zr–8Sn, Osseointegration, Osteoimmunomodulation, Anodic Oxidation, Strontium.*

INTRODUCTION

Matching the elastic modulus of oral implants and peri-implant bone is the premise of successful implantation [1]. The elastic modulus of Ti–24Nb–4Zr–8Sn (Ti2448, 49 GPa) is comparatively lower than that of current implant metal materials (pure titanium: 107 GPa and Ti6–Al–4V: 117 GPa) and is more suitable for oral implantation (bone cortex 20 GPa) [2, 3].

The osseointegration process involves a series of biological reactions, including the recruitment of multiple cells. Osteoblastic cells regulate osteogenesis by producing extracellular matrix (ECM) and controlling ECM mineralization. However, prior to osteogenesis, the inflammatory response induced by surrounding immune cells determines the *in vivo* fate of implants [4]. Briefly, osseointegration stems from an inflammation-modulated process in peri-implant bone tissue [5, 6].

Macrophages can be polarized by different stimuli. M1-type macrophages can release a series of proinflammatory cytokines [7, 8], while M2 macrophages secrete anti-inflammatory cytokines and can enhance ECM formation, mineralization, and osseointegration by secreting numerous mediators [9–11]. Accordingly, the M1/M2 type ratio of macrophages is pivotal for maintaining suitable osteoimmunology and the successful implantation of biomaterials.

Cell behaviors can be modulated by manipulating the surface morphology, elastic modulus, or chemical composition [12]. Accordingly, bioactive implants with appropriate surface physicochemical characteristics that can coordinate osteoimmunomodulation and consequently facilitate osseointegration are critical for the surface modification of dental implants.

*Authors to whom correspondence should be addressed.
Emails: drjiangw@163.com, Licuiying_67@163.com
†These two authors are co-first authors with equal contributions to the article.
Received: 1 July 2021
Revised/Accepted: 27 August 2021

Highly oriented nanotubes (NTs) possess unique electrical, optical, and biological properties [13–16]. In addition, these properties can be further enhanced by element doping [15, 17]. Bioactive ions can change the chemical composition and bioactivities of biomaterials [18, 19]. Strontium (Sr)-substituted bioactive materials can not only enhance osteogenesis and inhibit osteoclastogenesis but also coordinate osteoimmunomodulation [20, 22]. Some research has shown that Sr can antagonize the inflammatory effect of nuclear transcription factor-κB (NF-κB), indicating the anti-inflammatory effect of Sr on osteoclastogenesis [23, 24].

In this study, anodic oxidation (AO) and hydrothermal (HT) methods with adjustable parameters and stable procedures were used to fabricate Ti2-NTSr specimens. Then, we assessed the biological properties and osteogenic potential. The innovation of this study lies in the combination of the low elastic modulus and excellent osteogenic properties of these materials, which are more suitable for implantation, especially for patients with osteoporosis.

MATERIALS AND DETAILS

Specimens Fabrication and Characterization

Strontium-Dopped Nanotubes Fabrication

Machined commercial-grade 4 pure titanium (Ti-M) and Ti2448 alloy (Ti2-M) with appropriate diameters and thicknesses (1 mm in thickness, 10 mm in diameter) were fabricated for the following experiments. Prior to surface modification, the samples were ultrasonically cleaned. NTs on the Ti2448 surface were fabricated through an electrochemical process. Briefly, samples were placed in a two-electrode configuration containing a solution with NH_4F (0.15 mol/L) and $(NH_4)_2SO_4$ (1 mol/L) for 2 h at 30 V. The anodized Ti2448 specimens were labeled Ti2-NT. Then, some of the Ti2-NT samples were placed in solutions of $Sr(OH)_2 \cdot 8H_2O$ for 10 h at 180 °C [25]. These specimens were denoted Ti2-NTSr. Before biological evaluations, the specimens were steam sterilized.

Physical Characterization of the Specimens

The surface morphologies were detected by field-emission scanning electron microscopy (FE-SEM, SU8010, Hitachi, Japan) at 10 kV. The diameters of the nanotubes on Ti2-NTSr cross-sectional images of Ti2-NT and Ti2-NTSr were also measured by FE-SEM. The contents and distributions of Ti, Nb, Zr, Sn, O, and Sr were measured by energy dispersive spectrometry (EDS, QX200, Bruker, Germany). The chemical compositions were observed by X-ray photoelectron spectroscopy (XPS, Thermo, America). The wettability was measured by a drop shape analyzer (Kruss DSA100, Germany). The release of Sr in serum-free Dulbecco's Eagle medium (DMEM) on days 1, 3, 5, 7 and 14 was assessed by inductively coupled plasma-mass spectrometry (ICP-MS, PerkinElmer, USA). Then, the elemental distribution of Ti2-NTSr soaked for 14 days was analyzed by EDS. The zeta potentials of Ti2-NTSr from pH 7.0 to pH 8.4 were detected by a zeta potential analyzer (Zetasizer Nano ZS90, UK).

Osteogenic Properties of These Specimens

Osteoblast Culture of These Specimens

Osteoblasts (MC3T3-E1, Chinese Academy of Sciences, China) were cultivated in alpha-modified minimum essential medium (α-MEM, Gibco, USA) with 10% fetal bovine serum (FBS, Gibco, USA) at 100% humidity and 5% CO_2.

Proliferation and Cytoskeletal Assembly of Osteoblasts

The proliferation rates of osteoblasts cultured on the surface of these specimens on days 1, 3, 5, and 7 were detected by a CCK-8 assay. The cytoskeletal assembly and nuclei of osteoblasts were dyed with FITC-phalloidin (Sigma, USA) and 4,6-diamidino-2-phenylindole (DAPI, Sigma, USA), respectively. Briefly, osteoblasts (1×10^4 cells/cm^2) were divided into these four groups for 24 h. After rinsing and fixation, specimens with osteoblasts were dyed with phalloidin and DAPI. Then, cytoskeletal assembly was examined on a confocal laser fluorescence microscope (LSM710, Zeiss, Germany).

Osteogenesis

α-MEM with 10% FBS, b-glycerophosphate (10 mM), ascorbic acid (50 mg/ml), and dexamethasone (10 nM) was prepared to induce the osteogenic differentiation of osteoblasts. Then, ECM mineralization and alkaline phosphatase (ALP) assays were performed to assess osteogenesis. The transcription levels of osteogenic markers were measured by a real-time PCR (RT-PCR) device (Applied Biosystems, USA).

Seven days after osteogenic induction, the ALP activity in these four groups was assayed by an ALP kit (Njjcbio, China). Subsequently, the OD values were analyzed by a microplate reader instrument at 520 nm (PerkinElmer, Singapore).

Twenty-eight days after induction, 40 mM Alizarin Red (Sigma, America) reagent was used to assess ECM mineralization in these specimens. After rinsing and fixation, osteoblasts in these groups were incubated in the reagent and washed with ddH_2O. Stained results were captured. Then, Alizarin Red stain was dissolved in sodium phosphate (10 mM) and cetylpyridinium chloride (10%, Macklin, China) solutions, and the OD values (490 nm) of these solutions were recorded.

The transcription levels of early phenotypic markers for osteogenesis [*runt-related transcription factor-2* (*Runx-2*), *ALP*, *collagen type I* (*COL-1*), and *bone morphogenetic protein-2* (*BMP-2*)] on day 7 and terminal osteogenesis genes [*osteocalcin (OCN)*] on day 14 were detected by RT-PCR. The relevant primer sequences are shown in Table I.

Osteoimmunomodulatory Responses of Macrophages in the Specimens

Macrophage Cultivation

Macrophages (RAW 264.7, Chinese Academy of Sciences, China) were used in this research. After normal culture (DMEM with 10% FBS) for 24 h, macrophages were activated with lipopolysaccharide (LPS, 20 ng/mL) for 2 h.

Macrophage Morphology and Spreading

Macrophages (10^4/cm^2) were seeded on the specimens, and the morphology of macrophages was captured by FE-SEM after 24 h. The adhesion areas of all the cells on a randomly selected low-magnification field by SEM (400×) were analyzed and are shown as the means and standard deviations.

Polarization of Macrophages

Flow cytometry and immunofluorescence assays were adopted to assess the polarization of macrophages on different specimens 24 h after activation. Then, the fluorescence intensities (FITC-conjugated inducible nitric oxide synthase (iNOS); Tritc-conjugated arginase-1 (Arg-1)) of macrophages on these specimens were assessed by confocal laser fluorescence microscopy (LSM710, Zeiss, Germany). Macrophages (1×10^6) in these four groups were treated with APC-labeled CD206 antibody (BioLegend, USA) for flow cytometry assays (Beckman Coulter, USA).

The transcription levels of *CD206*, *interleukin-10 (IL-10)*, and *CD86*, the inflammatory genes *IL-6*, *iNOS*, *tumor necrosis factor-α* (*TNF-α*) and *IL-1β*, and the osteogenic genes *TGF-β1*, *VEGFA and BMP-2* were examined by RT-PCR on day 3. The relevant primers are in Table I.

The translational levels of IL-1β (Abcam, USA), CD86 (Proteintech, USA), TNF-α (Proteintech, USA), BMP-2 (CST, USA), IL-10 (Proteintech, USA), IL-6 (Abcam, USA), TGF-β1 (Proteintech, USA), iNOS (Proteintech, USA), and GAPDH (Proteintech, USA) were detected by western blots.

The Influence of Macrophage-Conditioned Medium on Osteoblasts

Osteoblast-Mediated Osteogenesis in Conditioned Medium

To prepare specimen-conditioned media, activated macrophages (10^4 cells/cm^2) were seeded onto specimens and cultivated in serum-free medium for 1 day. Then, these media were mixed with an equal volume of α-MEM and used as specimen-conditioned media.

After culture in specimen-conditioned medium (5% FBS) for 28 days, the ECM mineralization of osteoblasts was qualitatively and quantitatively measured by Alizarin Red staining.

Table I. Primer sequences used for RT-PCR.

Primer	Sequence (3′-5′)
GAPDH-F	TGATGGGTGTGAACCACGAG
GAPDH-R	CCCTTCCACGATGCCAAAGT
ALP-F	TGAGCGACACGGACAAGAAG
ALP-R	GCCTGGTAGTTGTTGTGAGCAT
Runx-2-F	AAATGCCTCCGCTGTTATGAA
Runx-2-R	GCTCCGGCCCACAAATCT
COL-1-F	CTCCGGCTCCTGCTCCTCTTA
COL-1-R	ACCAGGAAGTCCAGGCTGTC
OCN-F	CCGGGAGCAGTGTGAGCTTA
OCN-R	AGGCGGTCTTCAAGCCATACT
BMP-2-F	GCTCCACAAACGAGAAAAGC
BMP-2-R	AGCAAGGGGAAAAGGACACT
CD86-F	CTGCTCATCATTGTATGTCAC
CD86-R	ACTGCCTTCACTCTGCATTTG
IL-10-F	AGCCTTATCGGAAATGATCCAGT
IL-10-R	GGCCTTGTAGACACCTTGGT
CD206-F	AGACGAAATCCCTGCTACTG
CD206-R	CACCCATTCGAAGGCATTC
IL-1β-F	TGGAGAGTGTGGATCCCAAG
IL-1β-R	GGTGCTGATGTACCAGTTGG
IL-6-F	ATAGTCCTTCCTACCCCAATTTCC
IL-6-R	GATGAATTGGATGGTCTTGGTCC
iNOS-F	CACCAAGCTGAACTTGAGCG
iNOS-R	CGTGGCTTTGGGCTCCTC
TNF-α-F	CTGAACTTCGGGGTGATCGG
TNF-α-R	GGCTTGTCACTCGAATTTTGAGA
Arg-1-F	CTCCAAGCCAAAGTCCTTAGAG
Arg-1-R	AGGAGCTGTCATTAGGGACATC
VEGFA-F	GACTTGTGTTGGGAGGAGGA
VEGFA-R	TCTGGAAGTGAGCCAATGTG
TGF-β1-F	CAGTACAGCAAGGTCCTTGC
TGF-β1-R	ACGTAGTAGACGATGGGCAG

The Influence of Macrophages on Osteoblast Migration

Osteoblasts cultured in specimen-conditioned medium in a 6-well plate were prepared. A scratch was made across the center of each well when the confluence of the cells reached 90%. Subsequently, the cells in each well were rinsed to eliminate the nonadherent cells. The movement of cells toward the scratch was assessed at 0 h, 24 h, and 72 h. Then, the average migration distance was measured by ImageJ software.

Investigation of Osteointegration *In Vivo*

Animal Feeding

The animal experiment acquired the approval (LA2018233) of the Animal Research Committee of Peking University. Twenty Wistar rats (male, 10 weeks old; Weitonglihua, Beijing, China) were fed in a specific pathogen-free (SPF) facility, and water and a standard diet were available ad libitum.

Implant Placement and Tissue Preparation

Chloral hydrate (10%, 3 ml/kg, Leageng, China) was used in the current animal experiments for rat anesthesia. Forty holes (diameter: 2 mm), which were 5 mm from the

metaphysis of the bilateral distal femur of 20 rats, were prepared for implantation. Then, 40 implants of the four groups (2 mm diameter, 2.5 mm length) were inserted into the holes. Twelve hours or 2 weeks after surgery, the animals were sacrificed by deep anesthesia.

Investigation of Implant Biocompatibility

Twelve hours after surgery, 8 implants were removed from the holes in the rats under anesthesia. After fixation with 4% paraformaldehyde, the structure of the blood clot on the surface was evaluated by FE-SEM. The mean diameters of fibers and pores in the meshwork of blood clots on these four implants were measured by ImageJ. Two weeks after implantation, eight implant samples, 2 weeks after implantation, were extracted from the holes. The Ca and P depositions of the implants were tested by FE-SEM and EDS assays.

Hard Tissue Slices

Two weeks after implantation, 16 hard tissue sample sections were prepared. After fixation and resin embedding, bone tissues with the implants were sliced longitudinally with a section cutter. Sections (10 μm in thickness) were dyed with methylene blue/acid fuchsin. The implant-bone interface was evaluated by microscopy (Olympus, Japan). The bone-implant contacts (BICs%) of these sections were analyzed with Image-Pro Plus.

Statistical Analysis

All the data are shown as the mean $\pm$ standard deviation (SD). One-way ANOVA was performed using GraphPad Prism 8 (San Diego, USA). Values of $p < 0.05$ were considered as significant.

RESULTS

Surface Properties of the Samples

The surface and cross-sectional topographies of these groups were observed by FE-SEM and are shown in Figures 1 and 2. Stripes of Ti-M and Ti2-M were regularly distributed (Figs. 1(A(a–d))). After AO, nonregular NTs were fabricated on the Ti2448 surface at 30 V (Figs. 1(A(e, f))). The anodized Ti2448 surface had NTs with diameters of approximately 100 nm and lengths of 5 μm (Figs. 1(A(f)), 2(A)). The anodized surface was not flat, and some of the NTs bulged, while others sank. After HT treatment for 10 h, the Ti2-NTSr still maintained NT microstructures, which were similar to those of Ti2-NT (Figs. 1(A(e–h))).

The Sr content in the Ti2-NTSr group was 4.29% (Fig. 1(B(d))). The diameters of the nanotubes on Ti2-NTSr were approximately 100 nm (Fig. 1(A(h))). The content of O was substantially increased after anodization (Figs. 1(B(c, d))). The O content in Ti2-M was merely 5.35% (Fig. 1(B(b))) and increased to approximately 28.03% (Ti2-NT) (Fig. 1(B(c)))

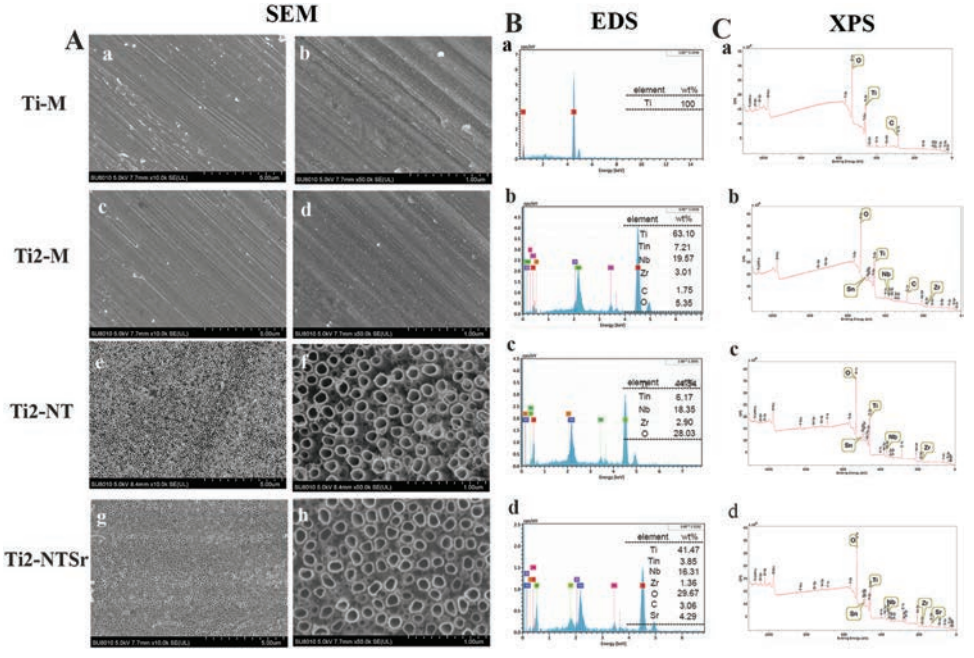

Figure 1. Characterization of the Ti-M, Ti2-M, Ti2-NT, and Ti2-NTSr groups. Surface morphologies (A) of Ti-M (a, b), Ti2-M (c, d), Ti2-NT (e, f), and Ti2-NTSr (g, h). Surface elemental contents (B) of Ti-M (a), Ti2-M (b), Ti2-NT (c), and Ti2-NTSr (d) determined by EDS elemental content assays. Surface element compositions by XPS analysis (C) of Ti-M (a), Ti2-M (b), Ti2-NT (c), and Ti2-NTSr (d).

and 29.67% (Ti2-NTSr) (Fig. 1(B(d))) after anodized oxidation.

The XPS spectra revealed that oxides were more abundant on the surfaces of the Ti2-NT and Ti2-NTSr specimens (Figs. 1(B(c, d)))) than on the surfaces of the Ti-M (Fig. 1(C(a))) and Ti2-M (Fig. 1(C(b))). Elemental oxides were analyzed, and the surface oxides of Ti2-NT were TiO_2, Nb_2O_5, ZrO_2, and SnO (Fig. 1(C(c))). As shown in Figures 1(C(d)), 2(D)), a well-defined Sr 3d core-level spectrum, ranging from 133 ± 0.5 eV to 135 ± 0.5 eV, was detected on the Ti2-NTSr sample [26].

The hydrophilicities of the Ti2-NTSr and Ti2-NT specimens were significantly higher than those of the Ti2-M and Ti-M specimens (Fig. 2(B)). The Sr release experiment (Fig. 2(C)) demonstrated that there was a burst of release on day 1, after which the release speed gradually declined. At day 14, the soaked Ti2-NTSr still contained 1.16 Wt% of Sr (Fig. 2(E)) on the surface, which indicated that the release of Sr on Ti2-NTSr specimens was a long-term process. The zeta potentials of Ti2-NTSr from pH 7.0 to pH 8.4 ranged from −21.5 mV to −22.5 mV (Fig. 2(F)).

Osteogenesis of Different Specimens

Adhesion and Proliferation of Osteoblasts

The CCK-8 assay demonstrated that osteoblasts continually proliferated on the surfaces of the four groups from day 1 to day 7 (Fig. 3(A)). The cell proliferation rate on Ti2-M was higher than that on Ti-M ($p < 0.05$). Then, the cell number decreased in the Ti2-NT and Ti2-NTSr groups compared with the Ti2-M group ($p < 0.05$).

After incubation for 24 h, osteoblasts fully spread on all specimens (Fig. 3(B)), and the cytoskeleton and nuclei were observed by laser fluorescence confocal microscopy. Osteoblasts on Ti-M and Ti2-M were regularly flattened, showing spindle morphology and growing along the striations, whereas cells on the Ti2-NT and Ti2-NTSr surfaces exhibited polygonal morphology and grew irregularly and spread out.

Osteogenic Differentiation and ECM Mineralization

Figure 3(C) shows that the ALP activities of the Ti2-NT and Ti2-NTSr specimens were significantly increased compared with those of the Ti-M and Ti2-M specimens ($p < 0.05$). Moreover, the ALP activity of the Ti2-NTSr group was much higher than that of the Ti2-NT group ($p < 0.05$). Figures 3(D), (E) shows that there were more ECM mineralized nodules in the Ti2-NTSr group than in the other three groups ($p < 0.05$).

Osteogenic-Related Genes of Osteoblasts in These Specimens

The transcription levels of osteogenic genes are shown in Figure 3(F). Compared with that on Ti-M, the expression of *COL-1*, *ALP*, *BMP-2* and *Runx-2* was specifically increased in the other groups, and the expression on Ti2-NTSr was the highest, which indicated the enhancement of osteoblast adhesion, osteogenic differentiation and secretion of bone matrix and the eventual stimulation of subsequent mineralization on Ti2-NTSr. In addition, the expression of the late-stage osteogenic gene *OCN* showed a similar trend.

Osteoimmunology of Different Specimens

Macrophage Adhesion and Spreading

Macrophages on Ti-M and Ti2-M specimens resembled polygonal stars and spread well with long filopodia, whereas the cells on Ti2-NTSr were round with

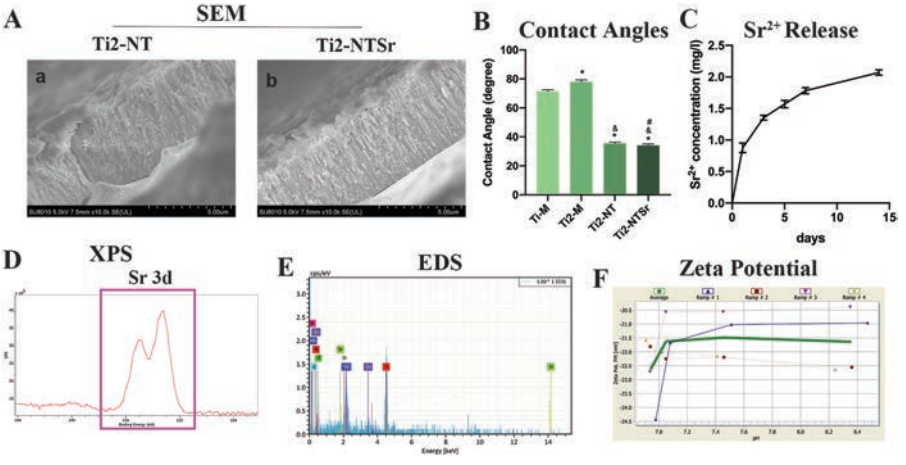

Figure 2. Cross-sectional images (A) of Ti2-NT (a) and Ti2-NTSr (b). Contact angles in the four groups (B). Sr release of Ti2-NTSr examined by ICP-MS on days 1, 3, 5, 7, and 14 (C). The binding energy of Sr on Ti2-NTSr as determined by XPS (D). An element content assay 14 days after Sr release was performed by EDS (E). Zeta potential of Ti2-NTSr (F). $^{*}p < 0.05$ versus Ti-M; $^{\&}p < 0.05$ versus Ti2-M; $^{\#}p < 0.05$ versus Ti2-NT.

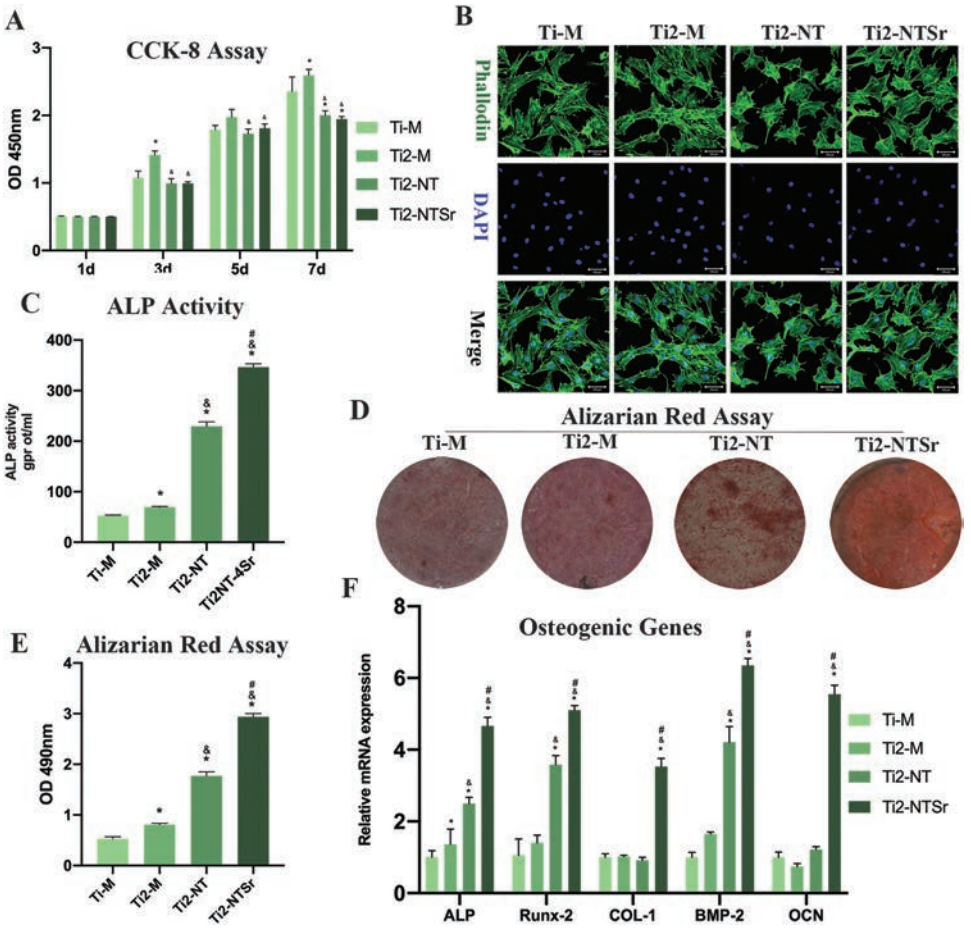

Figure 3. **Detection of osteogenic abilities in osteoblasts. Osteoblast proliferation on the surface in these four groups by CCK-8 assays (A). Cytoskeleton and nuclei of osteoblasts on the surfaces of these four specimens stained with FITC-phalloidin and DAPI (B), respectively. Images were observed at 40× magnification. ALP activity (C) of osteoblasts in these four samples. Qualitative (D) and quantitative (E) mineralization analysis of osteoblasts by Alizarin Red assay. Osteogenic-related gene expression in osteoblasts in these four samples (F). The data are shown as the mean ± SD. $^{*}p < 0.05$ versus Ti-M; $^{\&}p < 0.05$ versus Ti2-M; $^{\#}p < 0.05$ versus Ti2-NT.**

poor stretching (Fig. 4(A)). Cell adhesion area analysis (Fig. 4(B)) demonstrated that the mean spreading area of macrophages on the Ti-M specimen (108.3 ± 6.6 μm^2) was much larger than that on Ti2-NT (77.6 ± 5.5 μm^2, 0.71-fold, $p < 0.05$) and Ti2-NTSr (50.3 ± 3.5 μm^2, 0.45-fold, $p < 0.05$), whereas the spreading area on Ti2-M (106.9 ± 6.3 μm^2) was not significantly different ($p = 0.6267$).

Macrophage Polarization

Immunofluorescence and flow cytometry assays of macrophages demonstrated a higher percentage of M2-phenotype cells in the Ti2-NTSr group than in the other three groups (Figs. 4(C, D)). Moreover, the expression levels of M1-type markers (*CD86*) (Fig. 4(E)) and inflammatory cytokine genes (*IL-1*β, *iNOS*, *TNF-*α and *IL-6*) (Fig. 4(F)) were significantly decreased in the Ti2-NTSr samples. M2-type markers (*Arg-1* and *CD206*) (Figs. 4(E, F)), anti-inflammatory cytokine genes (*IL-10*) (Fig. 4(E)) and osteogenic genes (VEGFA, TGF-β1, and *BMP-2*) (Fig. 4(G)) were significantly enhanced. The translational levels of CD86, iNOS, IL-1β, TNF-α and IL-6 were also decreased ($p < 0.05$), while IL-10, TGF-β1 and BMP-2 were significantly increased ($p < 0.05$) in the Ti2-NTSr groups (Fig. 4(H)).

Coupling Effect of Osteoimmunomodulation with Osteogenesis

Osteoblast Recruitment

Figure 5(A) illustrates that the closure rates on Ti2-M ($7.2 \pm 1.2\%$, $p = 0.288$) and Ti2-NT ($6.9 \pm 0.9\%$, $p = 0.160$) were not obviously different from those on Ti-M ($9.1 \pm 1.6\%$), whereas the closure rate was significantly increased on Ti2-NTSr ($20.6 \pm 1.8\%$) at 24 h ($p < 0.05$). The closure rate in the Ti2-NTSr group ($70.4 \pm 2.6\%$) was increased compared with those in the machined and

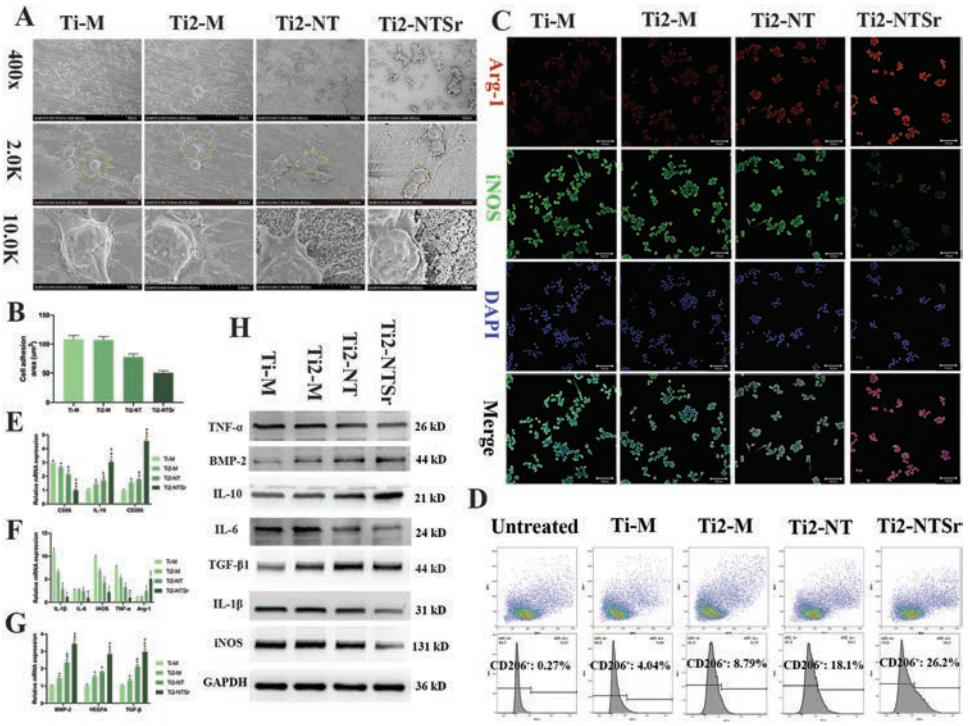

Figure 4. **Osteoimmunomodulatory ability assessment in macrophages. The adhesion and spreading of macrophages on these four samples detected by FE-SEM (A). Quantitative spreading areas of macrophages (B). Macrophage polarization in these four samples examined by laser confocal microscopy (C) and flow cytometric analysis (D). The expression levels of *CD86*, *CD206*, *IL-10* (E), *IL-1β*, *IL-6*, *iNOS*, TNF-α and *Arg-1* (F) and *BMP-2*, *VEGFA*, and *TGF-β* (G) were examined by RT-PCR. Translational levels of CD86, TNF-α, BMP-2, IL-10, IL-6, TGF-β, IL-1β, and iNOS (H) by Western blot. The data are shown as the mean ± SD. $^{*}p < 0.05$ versus Ti-M; $^{\&}p < 0.05$ versus Ti2-M; $^{\#}p < 0.05$ versus Ti2-NT.**

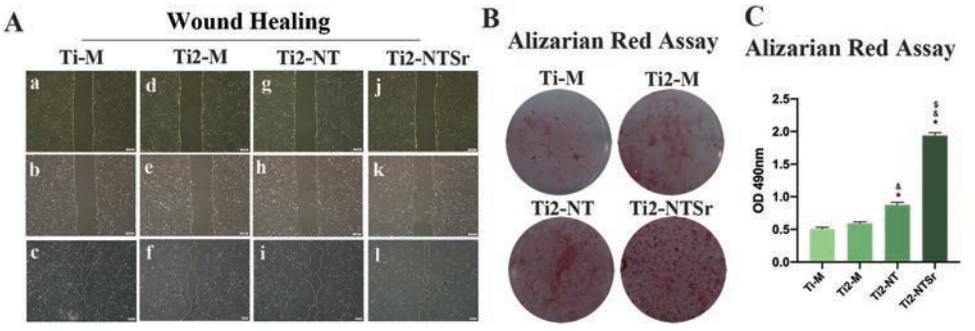

Figure 5. **Effects of specimen-conditioned macrophage media on osteogenesis induction. The effect of specimen-conditioned macrophage medium on osteoblast migration (A). Qualitative (B) and quantitative (C) mineralization analyses of osteoblasts in specimen-conditioned macrophage media. The values are shown as the mean ± SD. $^{*}p < 0.05$ versus Ti-M; $^{\&}p < 0.05$ versus Ti2-M; $^{\#}p < 0.05$ versus Ti2-NT.**

anodized groups (Ti2-M, 50.8 ± 1.9%; Ti2-NT, 55.1 ± 2.3%; Ti-M group 54.2 ± 2.1%) (Fig. 5(A)) at 72 h ($p < 0.05$).

Immunomodulation of Osteogenesis

Qualitative Alizarin Red analysis (Fig. 5(B)) showed that more ECM mineralized nodules were formed in Ti2-NTSr-specific conditioned medium on day 28, and the quantitative analysis supported this result (Fig. 5(C)). Specifically, compared with that in the Ti-M group, ECM mineralization on Ti2-NT (1.7-fold) and Ti2-NTSr (3.8-fold) was significantly enhanced ($p < 0.05$).

Investigation of Osseointegration *In Vivo*

Figure 6(A) shows the surface of the screwed-out Ti2-NTSr implant after surgery. The bottom surface of the implant, where the NT coating was still intact, was covered with fibrous tissue. The fibrous structure of the blood clot on Ti2-NTSr was thinner and denser than that on other specimens, with more cells attached to it. In

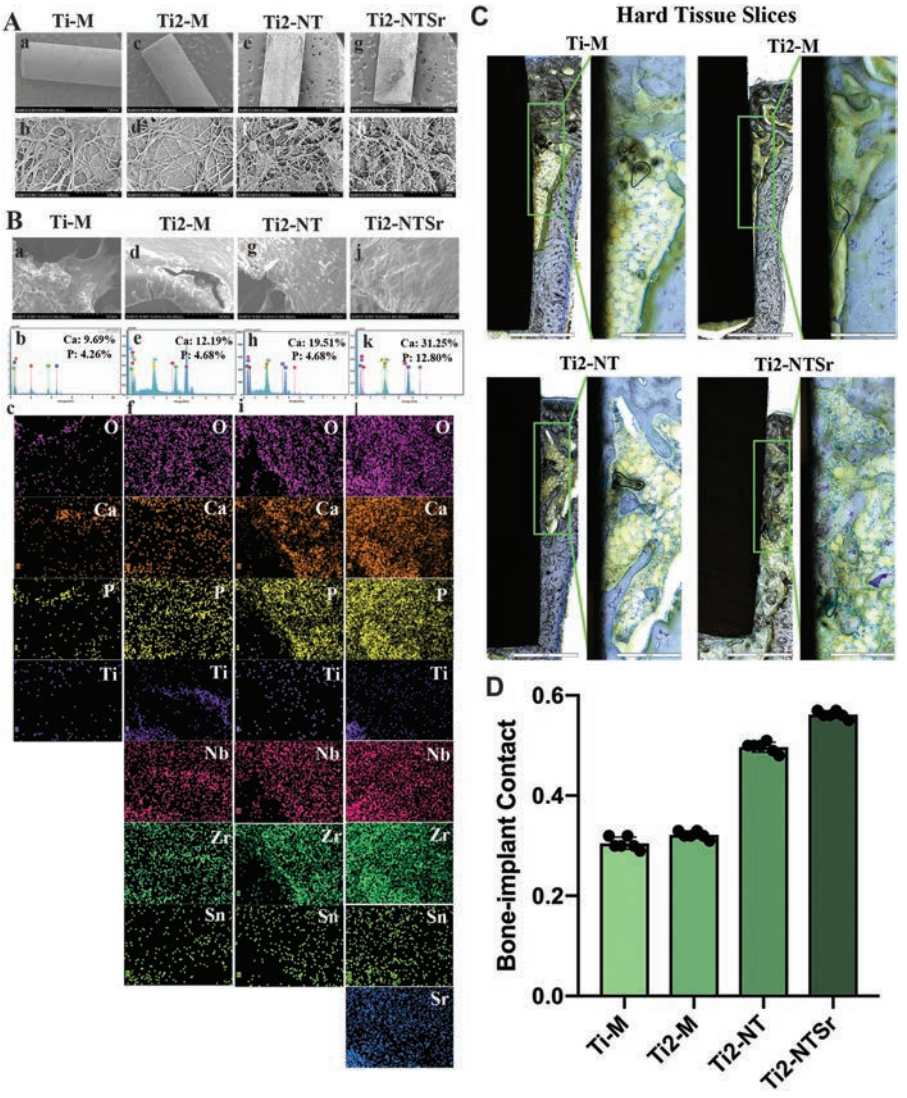

Figure 6. Osseointegration assessment *in vivo*. The images of implants 12 h after implantation were collected by SEM (A). The depositions of Ca and P on implants 2 weeks after implantation (B). Images of hard tissue slices (C) and BIC% (D) of these four groups.

contrast, the fibrous structures on pure Ti-M and Ti2-M were sparse with large pores. The depositions of Ca and P elements in the Ti2-NTSr group (Fig. 6(B)) were approximately 31.25% and 12.80%, respectively, which were much higher than those of the Ti-M (Ca: 9.69%, P: 4.26%), Ti2-M (Ca: 12.19%, P: 4.68%) and Ti2-NT (Ca: 19.51%, P: 4.68%) groups. Both the qualitative (Figs. 6(B(b, e, h, k))) and quantitative assays (Figs. 6(B(c, f, i, l))) of Ca and P showed the superior biocompatibility of Ti2-NTSr implants.

Hard tissue images (Fig. 6(C)) showed abundant newly formed woven bone and a higher BIC% (Fig. 6(D)) surrounding the implants in the Ti2-NT (49.67 ± 0.94) and Ti2-NTSr groups (56.17 ± 0.69), while less newly formed bone and a lower BIC% were detected in the Ti-M (28.50 ± 1.10) and Ti2-M (32.17 ± 0.69) groups.

DISCUSSION

The bone-implant surface is the exact point at which cells activate intracellular responses that initiate the following autocrine and paracrine procedures. Many cells, proteins, and mediators are involved in interactive processes [23, 27–31]. Thus, surface microtopography and element compositions determine downstream reactions [32]. Compared with microarc oxidation (MAO) and sandblasted large-grit acid-etched (SLA) modification, NT structures endowed Ti2448 alloy with better osteogenic ability [27]. Sr has a dose-dependent effect on bone metabolism. High-dose Sr (>10 At%) undermines bone formation, and low-dose Sr (1–7 At%) is conducive to osteogenesis [33, 34]. In our work, the content of Sr on the surface of Ti2-NTSr was approximately 1.51 At%, which is beneficial and safe for osteogenesis.

The EDS results demonstrated that Sr was well embedded on Ti2-NTSr. In addition, the AO procedure increased the presence of oxides. Oxides of biomaterials can alter the signal transduction of osteoblasts, changing the adhesion and extension of cells [35, 36] and subsequently enhancing osteogenic differentiation, which is conducive to osseointegration.

Osteoblast proliferation analysis of osteoblasts showed that materials with Ti2-NT or Ti2-NTSr layers caused compromised proliferation compared with Ti-M and Ti2-M. It has been reported that Sr- and Sr-containing biomaterials can increase the proliferation and initial attachment of osteoblasts [37, 38], whereas some studies have shown that Sr barely has an impact on the initial adhesion of osteoblasts [17, 39, 40]. In this study, the difference in cell proliferation between the Ti2-NTSr and Ti2-NT groups was not significant, indicating that Sr is not the decisive factor in proliferation in the current study. Note that the micromorphologies of the surface in the Ti2-NTSr and Ti2-NT groups were similar (Fig. 1), and it is conceivable that the regulation of osteoblast proliferation may be primarily due to surface morphology.

A stiff and well-spread actin cytoskeleton in osteoblasts is a prerequisite for good osteogenic differentiation, and the roughened surface of Ti2-NTSr can simulate the architecture of collagen fibrils in bone tissue and offer a more proper microtopography for osteogenesis [41, 42]. Sr, even at low concentrations, could markedly stimulate osteogenesis and compromise bone resorption via many pathways, including upregulating the expression of MAPK and the endogenous BMP-2 pathway [17, 43]. In this study, early osteogenesis-related and late-stage genes were similarly upregulated in this group. In particular, Runx-2, which was significantly upregulated in the Ti2-NTSr group, is a target of the BMP-2/TGF-β1 signaling pathway and a vital regulator of osteoblast differentiation [44, 45]. Thus, the results showed enhanced early osteogenesis and late mineralization in the Ti2-NTSr group in comparison with the other groups, which supported our hypothesis that Ti2-NTSr can facilitate osseointegration *in vivo*.

Immune cells are indispensable during the whole process of osteogenesis. Macrophages, as pivotal manipulators of osteoimmunomodulation and osseointegration processes, are indispensable during osseointegration [46, 47]. Most macrophages undergoing early-stage osseointegration are M1 macrophages, and a well-timed shift from M1-type to M2-type macrophages is pivotal to initiate new bone formation, while a prolonged M1 phase generates fibrous tissues around the implant and compromises osseointegration.

Sr can exert immunomodulatory effects, providing a suitable microenvironment for enhancing bone formation [20, 21]. The compositions and surface topographies of biomaterials manipulate the behaviors of macrophages by affecting their cytoskeleton [48]. Coating with improper nanostructures and compositions can stretch macrophages and facilitate adhesion and extension, inducing M1 polarization and intensifying osteoimmune responses by generating adverse cell adsorption forces. In contrast, an appropriate layer can undermine the proliferation and extension of macrophages, thus attenuating the osteoimmune response [49]. Additionally, hydrophobic materials tend to improve macrophage adhesion, enhancing the immune reaction [50], while hydrophilic surfaces inhibit macrophage adhesion. In our study, the hydrophilic Ti2-NTSr structure endowed the Ti2448 alloy with the ability to reduce macrophage spreading, significantly downregulate the transcription levels of *TNF-*α, *IL-*1β, and *IL-6*, and upregulate the expression of anti-inflammatory genes (*IL-10*) and osteogenic genes (*TGF-*β1, *VEGFA*, and *BMP-2)*. TGF-β1 and BMP-2 are involved in multiple biological processes, including osteogenesis activation. VEGFA can promote osteoblast differentiation synergistically with BMP-2 [51]. Some studies have found that the elastic modulus can modulate macrophage behavior [8]. However, Ti2-M exerted no significant regulatory effect compared with Ti-M. Thus, the behaviors of macrophages may be mainly determined by the surface micromorphology and addition of bioactive elements to specimens.

As a complicated process, osteogenesis requires the participation of multiple cells and mediators, which are necessary throughout osseointegration [31, 52]. The recruitment of osteoblasts to the implant-tissue surface is indispensable for the formation of bone mass. Activated M2 macrophages can produce various cytokines, including TGF-β1 and PDGF-BB, which can accelerate the bone reconstruction process by recruiting osteoblasts and some tissue-specific cells toward the bone implant surface [31, 49]. Ti2-NTSr-conditioned medium exhibited a strong capacity to recruit osteoblasts. The ECM mineralization assay also showed significant enhancement of osteogenesis in the Ti2-NTSr group. Ideally, Ti2-NTSr-coated Ti2448 material can recruit osteoblasts and then induce their differentiation.

In vivo, the formation of blood clots on implants initiates osseointegration [47], which is followed by the activation of platelets. Studies have shown that the fibers of clots are thinner and denser when platelets are activated [53–55]. Dense clots with abundant branchy and thin fibers are more rigid and can recruit more cells and proteins to the vicinity of the clot, which will accelerate bone formation around the implant. The clots on the surface of Ti2-NT and Ti2-NTSr were thin, compact three-dimensional collagen networks with smaller pores. The Ca and P contents of Ti2-NTSr were much higher than the depositions of the other groups, which strongly exhibited the favorable biocompatibility of Ti2-NTSr specimens. Furthermore, the BIC% of the Ti2-NTSr implant was much higher than that of the other groups ($p < 0.05$), which demonstrated the superior osseointegration of Ti2-NTSr-coated implants *in vivo*.

CONCLUSION

In this study, we successfully fabricated a newly developed Ti2-NTSr coating on a Ti2448 alloy by anodization and HT processes. The Ti2-NTSr coating also possessed excellent biocompatibility. The present study showed that the Ti2-NTSr coating could improve osteogenic functions, induce favorable osteoimmunomodulation and enhance osseointegration. In conclusion, a Ti2448 alloy with a Ti2-NTSr coating is conducive to osseointegration and has potential for clinical applications.

Ethical Compliance

The animal experiments in the research obtained approval from the Animal Research Committee of Peking University (LA2018233), and all the procedures in the animal experiments were conducted following the protocols and legal and ethical standards required for animals.

Conflicts of Interest Declaration

All authors declare that there are no conflicts of interest related to this paper.

Acknowledgments: This work was funded by the "Touyan" Project of Heilongjiang Province of China and the National Key Research and Development Program of China (2016YFC1102603).

REFERENCES

1. Brizuela, A., Herrero-Climent, M., Rios-Carrasco, E., Rios-Santos, J.V., Perez, R.V., Manero, J.M. and Gil Mur, J., **2019**. Influence of the elastic modulus on the osseointegration of dental implants. *Materials (Basel)*, *12*(6), p.980.
2. Nune, K.C., Misra, R.D.K., Li, S.J., Hao, Y.L. and Yang, R., **2017**. Osteoblast cellular activity on low elastic modulus Ti–24nb–4Zr–8Sn alloy. *Dental Materials*, *33*(2), pp.152–165.
3. Nune, K.C., Misra, R.D., Li, S.J., Hao, Y.L. and Yang, R., **2017**. Cellular response of osteoblasts to low modulus Ti–24Nb–4Zr–8Sn alloy mesh structure. *Journal of Biomedical Materials Research Part A*, *105*(3), pp.859–870.
4. Vishwakarma, A., Bhise, N.S., Evangelista, M.B., Rouwkema, J., Dokmeci, M.R., Ghaemmaghami, A.M., Vrana, N.E. and Khademhosseini, A., **2016**. Engineering immunomodulatory biomaterials to tune the inflammatory response. *Trends in Biotechnology*, *34* (6), pp.470–482.
5. Takayanagi, H., **2007**. Osteoimmunology: Shared mechanisms and crosstalk between the immune and bone systems. *Nature Reviews Immunology*, *7*(4), pp.292–304.
6. Chen, Z., Klein, T., Murray, R.Z., Crawford, R., Chang, J., Wu, C. and Xiao, Y., **2016**. Osteoimmunomodulation for the development of advanced bone biomaterials. *Materials Today*, *19*(6), pp.304–321.
7. Abumaree, M.H., Al Harthy, S., Al Subayyil, A.M., Alshabibi, M.A., Abomaray, F.M., Khatlani, T., Kalionis, B., El-Muzaini, M.F., Al Jumah, M.A., Jawdat, D., Alawad, A.O. and AlAskar, A.S., **2019**. Decidua basalis mesenchymal stem cells favor inflammatory M1 macrophage differentiation in vitro. *Cells*, *8*(2), p.173.
8. Veremeyko, T., Yung, A.W.Y., Anthony, D.C., Strekalova, T. and Ponomarev, E.D., **2018**. Early growth response gene-2 is essential for M1 and M2 macrophage activation and plasticity by modulation of the transcription factor CEBPbeta. *Frontiers in Immunology*, *9*, p.2515.
9. Sridharan, R., Cameron, A.R., Kelly, D.J., Kearney, C.J. and O'Brien, F.J., **2015**. Biomaterial based modulation of macrophage polarization: A review and suggested design principles. *Materials Today*, *18*(6), pp.313–325.
10. Wang, Q., He, Z., Huang, M., Liu, T., Wang, Y., Xu, H., Duan, H., Ma, P., Zhang, L., Zamvil, S.S., Hidalgo, J., Zhang, Z., O'Rourke, D.M., Dahmane, N., Brem, S., Mou, Y., Gong, Y. and Fan, Y., **2018**. Vascular niche IL-6 induces alternative macrophage activation in glioblastoma through HIF-2alpha. *Nature Communications*, *9*(1), p.559.
11. Alvarado-Vazquez, P.A., Bernal, L., Paige, C.A., Grosick, R.L., Moracho Vilrriales, C., Ferreira, D.W., Ulecia-Moron, C. and Romero-Sandoval, E.A., **2017**. Macrophage-specific nanotechnology-driven CD163 overexpression in human macrophages results in an M2 phenotype under inflammatory conditions. *Immunobiology*, *222*(8–9), pp.900–912.
12. Li, Y., Xiao, Y. and Liu, C., **2017**. The horizon of materiobiology: A perspective on material-guided cell behaviors and tissue engineering. *Chemical Reviews*, *117*(5), pp.4376–4421.
13. Wang, X., Mei, L., Jin, M., Jiang, X., Li, X., Li, J., Xu, Y., Meng, Z., Zhu, J. and Wu, F., **2021**. Composite coating of graphene oxide/TiO_2 nanotubes/HHC-36 antibacterial peptide construction and an exploration of its bacteriostat and osteogenesis effects. *Journal of Biomedical Nanotechonology*, *17*, pp.662–676.
14. Attarilar, S., Djavanroodi, F., Ebrahimi, M., Al-Fadhalah, K.J., Wang, L. and Mozafari, M., **2021**. Hierarchical microstructure tailoring of pure titanium for enhancing cellular response at tissue-implant interface. *Journal of Biomedical Nanotechnology*, *17*, pp.115–130.
15. Zhang, X., Zhang, X., Wang, B., Lan, J., Yang, H., Wang, Z., Chang, X., Wang, S., Ma, X., Qiao, H., Lin, H., Han, S. and Huang, Y., **2020**. Synergistic effects of lanthanum and strontium to enhance the osteogenic activity of TiO_2 nanotube biological interface. *Ceramics International*, *46*(9), pp.13969–13979.
16. Lee, Y., Bhattarai, G., Park, I., Kim, G.R., Kim, G.E., Lee, M. and Yi, H., **2013**. Bone regeneration around N-acetyl cysteine-loaded nanotube titanium dental implant in rat mandible. *Biomaterials*, *34*(38), pp.10199–10208.
17. Zhao, L., Wang, H., Huo, K., Zhang, X., Wang, W., Zhang, Y., Wu, Z. and Chu, P.K., **2013**. The osteogenic activity of strontium loaded titania nanotube arrays on titanium substrates. *Biomaterials*, *34*(1), pp.19–29.
18. Shi, M., Chen, Z., Farnaghi, S., Friis, T., Mao, X., Xiao, Y. and Wu, C., **2016**. Copper-doped mesoporous silica nanospheres, a promising immunomodulatory agent for inducing osteogenesis. *Acta Biomaterialia*, *30*, pp.334–344.
19. Wu, C. and Chang, J., **2014**. Multifunctional mesoporous bioactive glasses for effective delivery of therapeutic ions and drug/growth factors. *Journal of Controlled Release*, *193*, pp.282–295.
20. Kargozar, S., Montazerian, M., Fiume, E. and Baino, F., **2019**. Multiple and promising applications of strontium (Sr)-containing bioactive glasses in bone tissue engineering. *Frontiers in Bioengineering and Biotechnology*, *7*, p.161.
21. Zhang, W., Zhao, F., Huang, D., Fu, X., Li, X. and Chen, X., **2016**. Strontium-substituted submicrometer bioactive glasses modulate macrophage responses for improved bone regeneration. *ACS Applied Materials & Interfaces*, *8*(45), pp.30747–30758.
22. Liu, J., Rawlinson, S.C., Hill, R.G. and Fortune, F., **2016**. Strontium-substituted bioactive glasses in vitro osteogenic and antibacterial effects. *Dental Materials*, *32*(3), pp.412–422.
23. Loi, F., Córdova, L.A., Zhang, R., Pajarinen, J., Lin, T., Goodman, S.B. and Yao, Z., **2016**. The effects of immunomodulation by macrophage subsets on osteogenesis in vitro. *Stem Cell Research & Therapy*, *7*(1), p.15.

24. Chen, Z., Klein, T., Murray, R.Z., Crawford, R., Chang, J., Wu, C. and Xiao, Y., **2016**. Osteoimmunomodulation for the development of advanced bone biomaterials. *Materials Today*, *19*(6), pp.304–321.

25. De Bonis, A., Uskokovic, V., Barbaro, K., Fadeeva, I., Curcio, M., Imperatori, L., Teghil, R. and Rau, J.V., **2020**. Pulsed laser deposition temperature effects on strontium-substituted hydroxyapatite thin films for biomedical implants. *Cell Biology and Toxicology*, *36*(6), pp.537–551.

26. Zhang, W., Cao, H., Zhang, X., Li, G., Chang, Q., Zhao, J., Qiao, Y., Ding, X., Yang, G., Liu, X. and Jiang, X., **2016**. A strontium-incorporated nanoporous titanium implant surface for rapid osseointegration. *Nanoscale*, *8*(9), pp.5291–5301.

27. Zhan, X., Li, S., Cui, Y., Tao, A., Wang, C., Li, H., Zhang, L., Yu, H., Jiang, J. and Li, C., **2020**. Comparison of the osteoblastic activity of low elastic modulus Ti–24Nb–4Zr–8Sn alloy and pure titanium modified by physical and chemical methods. *Materials Science & Engineering C-Materials for Biological Applications*, *113*, p.111018.

28. Andrukhov, O., Huber, R., Shi, B., Berner, S., Rausch-Fan, X., Moritz, A., Spencer, N.D. and Schedle, A., **2016**. Proliferation, behavior, and differentiation of osteoblasts on surfaces of different microroughness. *Dental Materials*, *32*(11), pp.1374–1384.

29. Annamalai, R.T., Turner, P.A., Carson, W.F., Levi, B., Kunkel, S. and Stegemann, J.P., **2018**. Harnessing macrophage-mediated degradation of gelatin microspheres for spatiotemporal control of BMP2 release. *Biomaterials*, *161*, pp.216–227.

30. An, J., Yang, H., Zhang, Q., Liu, C., Zhao, J., Zhang, L. and Chen, B., **2016**. Natural products for treatment of osteoporosis: The effects and mechanisms on promoting osteoblast-mediated bone formation. *Life Sciences*, *147*, pp.46–58.

31. Chen, Z., Mao, X., Tan, L., Friis, T., Wu, C., Crawford, R. and Xiao, Y., **2014**. Osteoimmunomodulatory properties of magnesium scaffolds coated with beta-tricalcium phosphate. *Biomaterials*, *35*(30), pp.8553–8565.

32. Franz, S., Rammelt, S., Scharnweber, D. and Simon, J.C., **2011**. Immune responses to implants—A review of the implications for the design of immunomodulatory biomaterials. *Biomaterials*, *32*(28), pp.6692–6709.

33. Gong, Z., Cheng, H., Zhang, M., Liu, X., Zeng, Y., Xiang, K., Xu, Y., Wang, Y. and Zhu, Z., **2017**. Osteogenic activity and angiogenesis of a srtio3 nano-gridding structure on titanium surface. *Journal of Materials Chemistry B*, *5*(3), pp.537–552.

34. Denry, I., Goudouri, O., Fredericks, D.C., Akkouch, A., Acevedo, M.R. and Holloway, J.A., **2018**. Strontium-releasing fluorapatite glass-ceramic scaffolds: Structural characterization and in vivo performance. *Acta Biomaterialia*, *75*, pp.463–471.

35. Thian, E.S., Huang, J., Ahmad, Z., Edirisinghe, M.J., Jayasinghe, S.N., Ireland, D.C., Brooks, R.A., Rushton, N., Best, S.M. and Bonfield, W., **2008**. Influence of nanohydroxyapatite patterns deposited by electrohydrodynamic spraying on osteoblast response. *Journal of Biomedical Materials Research Part A*, *85*(1), pp.188–194.

36. Galli, C., Piemontese, M., Lumetti, S., Ravanetti, F., Macaluso, G.M. and Passeri, G., **2012**. Actin cytoskeleton controls activation of Wnt/β-catenin signaling in mesenchymal cells on implant surfaces with different topographies. *Acta Biomaterialia*, *8*(8), pp.2963–2968.

37. Zhang, J., Zhao, S., Zhu, Y., Huang, Y., Zhu, M., Tao, C. and Zhang, C., **2014**. Three-dimensional printing of strontium-containing mesoporous bioactive glass scaffolds for bone regeneration. *Acta Biomaterialia*, *10*(5), pp.2269–2281.

38. Panzavolta, S., Torricelli, P., Sturba, L., Bracci, B., Giardino, R. and Bigi, A., **2008**. Setting properties and in vitro bioactivity of strontium-enriched gelatin–calcium phosphate bone cements. *Journal of Biomedical Materials Research Part A*, *84*(4), pp.965–972.

39. Park, J.W., Kim, H.K., Kim, Y.J., Jang, J.H., Song, H. and Hanawa, T., **2010**. Osteoblast response and osseointegration of a Ti-6Al-4V alloy implant incorporating strontium. *Acta Biomaterialia*, *6*(7), pp.2843–2851.

40. Zhou, C., Xu, A., Wang, D., Lin, G., Liu, T. and He, F., **2018**. The effects of Sr-incorporated micro/nano rough titanium surface on rBMSC migration and osteogenic differentiation for rapid osseointegration. *Biomaterials Science*, *6*(7), pp.1946–1961.

41. Cheng, H., Xiong, W., Fang, Z., Guan, H., Wu, W., Li, Y., Zhang, Y., Alvarez, M.M., Gao, B., Huo, K., Xu, J., Xu, N., Zhang, C., Fu, J., Khademhosseini, A. and Li, F., **2016**. Strontium (Sr) and silver (Ag) loaded nanotubular structures with combined osteoinductive and antimicrobial activities. *Acta Biomaterialia*, *31*, pp.388–400.

42. Li, Y., Qi, Y., Gao, Q., Niu, Q., Shen, M., Fu, Q., Hu, K. and Kong, L., **2015**. Effects of a micro/nano rough strontium-loaded surface on osseointegration. *International Journal of Nanomedicine*, *10*, pp.4549–4563.

43. Zhang, W., Tian, Y., He, H., Chen, R., Ma, Y., Guo, H., Yuan, Y. and Liu, C., **2016**. Strontium attenuates rhBMP-2-induced osteogenic differentiation via formation of Sr-rhBMP-2 complex and suppression of smad-dependent signaling pathway. *Acta Biomaterialia*, *33*, pp.290–300.

44. Wei, J., Shimazu, J., Makinistoglu, M.P., Maurizi, A., Kajimura, D., Zong, H., Takarada, T., Iezaki, T., Pessin, J.E., Hinoi, E. and Karsenty, G., **2015**. Glucose uptake and runx2 synergize to orchestrate osteoblast differentiation and bone formation. *Cell*, *161*(7), pp.1576–1591.

45. Jang, W., Kim, E.J., Bae, I., Lee, K., Kim, Y.D., Kim, D., Kim, S., Lee, C., Franceschi, R.T., Choi, H. and Koh, J., **2011**. Metformin induces osteoblast differentiation via orphan nuclear receptor SHP-mediated transactivation of runx2. *Bone*, *48*(4), pp.885–893.

46. Brown, B.N., Ratner, B.D., Goodman, S.B., Amar, S. and Badylak, S.F., **2012**. Macrophage polarization: An opportunity for improved outcomes in biomaterials and regenerative medicine. *Biomaterials*, *33*(15), pp.3792–3802.

47. Bai, L., Du, Z., Du, J., Yao, W., Zhang, J., Weng, Z., Liu, S., Zhao, Y., Liu, Y., Zhang, X., Huang, X., Yao, X., Crawford, R., Hang, R., Huang, D., Tang, B. and Xiao, Y., **2018**. A multifaceted coating on titanium dictates osteoimmunomodulation and osteo/angio-genesis towards ameliorative osseointegration. *Biomaterials*, *162*, pp.154–169.

48. Rice, J., Hunt, J., Gallagher, J., Hanarp, P., Sutherland, D. and Gold, J., **2003**. Quantitative assessment of the response of primary derived human osteoblasts and macrophages to a range of nanotopography surfaces in a single culture model in vitro. *Biomaterials*, *24*, pp.4799–4818.

49. Chen, L., Wang, D., Peng, F., Qiu, J., Ouyang, L., Qiao, Y. and Liu, X., **2019**. Nanostructural surfaces with different elastic moduli regulate the immune response by stretching macrophages. *Nano Letters*, *19*(6), pp.3480–3489.

50. Hezi-Yamit, A., Sullivan, C., Wong, J., David, L., Chen, M., Cheng, P., Shumaker, D., Wilcox, J.N. and Udipi, K., **2009**. Impact of polymer hydrophilicity on biocompatibility: Implication for DES polymer design. *Journal of Biomedical Materials Research Part A*, *90*, pp.133–141.

51. Peng, H., Usas, A., Gearhart, B. and Huard, J., **2004**. VEGF enhances bone formation and bone healing elicited by transduced muscle-derived stem cells expressing human BMP2. *Molecular Therapy*, *9*, p.S337.

52. Pajarinen, J., Lin, T., Gibon, E., Kohno, Y., Maruyama, M., Nathan, K., Lu, L., Yao, Z. and Goodman, S.B., **2019**. Mesenchymal stem cell-macrophage crosstalk and bone healing. *Biomaterials*, *196*, pp.80–89.

53. Chandrashekar, A., Singh, G., Jonah, G., Sikalas, N. and Labropoulos, N., **2018**. Mechanical and biochemical role of fibrin within a venous thrombus. *European Journal of Vascular and Endovascular Surgery*, *55*, pp.417–424.

54. Silva, G.A.F., Faot, F., da Silva, W.J. and Del Bel Cury, A.A., **2021**. Does implant surface hydrophilicity influence themaintenance of surface integrity after insertioninto low-density artificial bone? *Dental Materials*, *37*, pp.e69–e84.

55. Kopf, B.S., Ruch, S., Berner, S., Spencer, N.D. and Maniura-Weber, K., **2015**. The role of nanostructures and hydrophilicity in osseointegration: In-vitro protein-adsorption and blood-interaction studies. *Journal of Biomedical Materials Research Part A*, *103*, pp.2661–2672.